CONF-780554-1

LA-UR -78-1205

TITLE: Investigation of the Microdosimetric Characteristics of Broad, Therapeutic Beams of Negative Pions at LAMPF

AUTHOR(S): J. F. Dicello and M. Zaider

SUBMITTED TO: 6th Symposium on Microdosimetry
Brussels, Belgium May 1978

MASTER

los alamos
scientific laboratory
of the University of California
LOS ALAMOS, NEW MEXICO 87544

An Affirmative Action/Equal Opportunity Employer

Form No. 836
St. No. 2629
1/75

UNITED STATES
ENERGY RESEARCH AND
DEVELOPMENT ADMINISTRATION
CONTRACT W-7405-ENG. 36

"Investigation of the Microdosimetric Characteristics of Broad, Therapeutic Beams of Negative Pions at LAMPF"

J. F. Dicello and M. Zaider
University of California
Los Alamos Scientific Laboratory
Los Alamos, New Mexico 87545

ABSTRACT

Preclinical human studies with negative pions are presently being conducted at the Clinton P. Anderson Meson Physics Facility (LAMPF) of the Los Alamos Scientific Laboratory. Presently, the proton current at LAMPF is 300 µA, average, and the instantaneous pion rate at the biomedical channel is about 2.4×10^7 pions/sec, cm^2. This corresponds to a dose rate of about 6 rad/min in a 1 liter volume. Conventional microdosimetric techniques are not applicable at these event-rates because of detector damage, gas breakdown, pileup and deadtime effects, and saturation of the electronics. A new microdosimetric system developed at LAMPF in order to overcome these problems is described.

Treatment fields as large as 17×17 cm^2 and as deep as 10 cm have been developed. The radiation quality of such pion beams is changing rapidly throughout the treatment volume. For this reason, microdosimetric data have been obtained for a broad, therapeutic beam (10 cm deep, 1 liter volume) as part of a continuing program to characterize those aspects of the radiation quality which produce changes in the biological response.

Microdosimetric data have been obtained at several positions along the central axis of the beam in the peak region. The characteristics of the broad, pion beams are discussed and are compared with those of a narrow pion beam, with neutron data, and with data for broad, heavy ion beams.

An attempt is made to calculate broad beam distributions from data for narrow beams for purposes of treatment planning, and the results are compared with the measured spectra.

INTRODUCTION

Preclinical trials on selected patients are currently being performed with negative pion beams at the Clinton P. Anderson Meson Physics Facility (LAMPF) of the Los Alamos Scientific Laboratory.[1] The potential therapeutic advantages of pions have been reviewed in the literature.[2] These can be summarized as follows: there is a substantial increase in the dose delivered by pions in the treatment region as compared with that delivered in the entrance region or the surrounding tissues. This improved dose localization along with good beam shaping could result in better tumor response with less deleterious effects to the surrounding tissue. Equally important is that a significant fraction of the dose in the region where the pions are stopping (the peak region) is delivered by high-Z nuclei which result from pion absorption by target nuclei (star byproducts). This increased concentration of energy deposited by these heavier particles sh uld result in higher relative biological effects (RBE) and lower oxygen enhancement ratios (OER) as compared to those obtained in the surrounding region. Changes in the type of secondary particles produced, their energies, and their spatial distribution throughout the treatment volume can alter the biological response. It is important that any comprehensive treatment plan includes an adequate characterization of the radiation quality throughout the treatment field. Microdosimetry studies play a major role in this respect.

The first microdosimetric spectra for negative pions were reported by Lucas, Quam, and Raju[3] for a beam used at Berkeley for radiobiological studies. Dicello, Fessenden, and Henkelman[2] have reviewed the microdosimetric characteristics of narrow pion beams, such as those used to irradiate superficial skin nodules.[1]

Recently, broad, therapeutic pion beams have been developed at LAMPF for larger treatment volumes. It is difficult to predict in a quantitative manner the radiation quality characteristics of these new beams. A systematic experimental and theoretical effort has been initiated at Los Alamos in order to determine the microdosimetric characteristics of these beams.

This paper presents microdosimetric spectra for a broad pion beam representative of those used in preclinical studies at LAMPF. A comparison is made between these results and those for a narrow beam and with similar data for heavy-ion and neutron beams. For comparative purposes values for the RBE and OER for a specific cell line have been calculated with the

Theory of Dual Radiation Action.(4)

II. EXPERIMENTAL PROCEDURE

The experiments reported in this paper were performed using pion beams at the biomedical channel at LAMPF. The beam consists of 76-MeV negative pions with a full width at half-maximum (FWHM) in energy of 4%. The percentage of electrons and muons in the beam is 12% and 12%, respectively.(5) The time structure of the beam is characterized by a macrostructure of 120 pulses per second, each one 500 μsec wide. The instantaneous pion rate is about 2.4×10^7 pions/sec cm^2 for a primary proton current of 300 μA, average, incident on a pyrolytic carbon target.

A schematic representation of the experimental setup is shown in Fig. 1. The pion beam enters the experimental room vertically and is incident on a large water phantom. The detector is placed in the water phantom at a distance of 100 cm from the effective downstream edge of the last quadrupole. A collimator of elliptical cross section, 9 x 11 cm^2, made of Cerrobend, is positioned at the water surface. A dynamically variable absorber(6) (range shifter) is placed in the pion beam in order to obtain dose distributions which are flat over a 10 cm depth along the beam axis. The sweep functions of the range shifter can be programmed and various range modulations can be achieved.(6)

A parallel-plate ionization chamber placed above the water phantom monitored the pion beam. A second beam monitor consisting of a plastic scintillator detector (0.5 cm thick, 2.54 cm diameter) was positioned at a variable distance with respect to the main axis of the beam.

The detector consists of a modified Rossi-type spherical proportional counter having an inner diameter of 2.5 cm. The sensitive volume is delimited by a tissue-equivalent plastic shell of 0.3-cm thickness. Electron multiplication occurs between a helix and the central wire (anode) which is ac-coupled to the input FET of a charge-sensitive preamplifier. The first stage of this low-noise ($\sim$ 150 e^- rms) preamplifier(7) is encased in the chamber base. The preamplifier was designed for low electronic noise and a wide dynamic range of amplitudes without distortion when a pulsed bias is applied to the detector. The bias voltage is applied to the outer shell of the counter and the helix. The ratio of the anode-to-helix potential was maintained at 5:4 by a divider network.

The counter gas was a mixture, by volume, of 55.0% C_3H_8, 39.6% CO_2, and 5.4% N_2. A regulated flow system was used to maintain gas purity, constant pressure (34 Torr), and constant flow rate in the detector.

As mentioned earlier in this paper, the high intensity of the pion beam at LAMPF (as much as 100 rad/min), necessary for therapeutical treatments, would normally be prohibitive for an in-beam counting experiment of the type reported here. The following approach was developed in order to perform measurements without changing the phase space or contamination of the beam. A low intensity beam pulse is generated in the injector once during every 10 macropulses. The intensity of this pulse can be further controlled through an electrostatic deflector (chopper plates) placed in the proton beam line. The average proton intensity is kept constant by increasing the instantaneous intensity of the remaining pulses. The present measurements were taken during the 1-in-10 pulses.

A direct consequence of this method of operation is the necessity of protecting the detector from high-voltage breakdown or electronic failure during the high intensity pulses, with the resulting malfunctioning during the low intensity pulses. For these reasons, the bias voltage on the shell is pulsed by a fast high-voltage reed relay such that, during the high intensity pulses, the shell and the helix are at the same potential. During data collection (approximately 400 μs, 12 times per second) the shell-to-helix voltage is reset to the normal values. Extensive tests made for both pulsed and unpulsed modes show that data obtained by the two methods are in agreement.

Analog pulses from the preamplifier are fed through a linear amplifier into an analog-to-digital converter and stored in the memory of a PDP-11/45 computer through a CAMAC interface. A state-of-the-art pile-up rejection system is used. This system allows variable time resolution and amplitude discrimination in order to accommodate various counting rates and energy ranges. In the present setup, more than 99.5% of the piled-up pulses are rejected. In order to measure the system deadtime, a precision pulser is used to simulate real energy depositions. The pulser is triggered by the beam pulses. The simulated events from the pulser are fed in the system through a capacitor to the input of the preamplifier. They pass through the same electronic system as any real event and are recorded in the spectrum as a separate peak. The integrated counts in this "pulser peak" divided by the number of pulser triggers is the fractional live-time in the system. The intensity of the 1-in-10 pulses was adjusted such that the overall deadtime was less than 15%.

The system was calibrated in energy by use of a collimated beam of Am^{241} alpha particles. A complete spectrum consisted of several overlapping segments, each covering a specific range of lineal energies. The segments were matched by use of data obtained with the beam monitoring system corrected for deadtime. The data were stored, analyzed, and matched to previously accumulated segments on-line on a PDP-11/45 computer with software developed for the present application.

III. RESULTS AND DISCUSSION

Microdosimetric spectra have been obtained for a broad, range-shifted beam which has a peak region of approximately 10 cm in length along the central axis of the beam. Two spectra obtained at 8 cm and 16 cm depths in the water phantom are shown in Fig. 2 in a yd(y) vs log y representation. Both curves have been normalized to unit dose. The positions where the distributions have been measured are indicated in the insert of Fig. 2 where the depth-dose curve for the present beam is shown.

The microdosimetric spectra shown in Fig. 2 have some characteristics which are common to all negative pion beams. These spectra include energy deposition contributions from the primary particles (pions, muons, and electrons) and from the reaction products resulting from in-flight and absorption processes. The energy deposited by the primary particles is centered around the average stopping power for each type of particle. As the particles penetrate into the phantom, their energy spectra become increasingly more complicated because of Coulomb and nuclear scattering effects. Other factors such as energy straggling, path length distribution in the detector and the statistical fluctuations of the ion-pair formation and multiplication processes will further spread the energy spectra. The average energy depositions for pions, muons, and electrons range from 280, 236, and 225 eV/μm, respectively, at the surface of the water phantom, to 3.68, 0.314, and 0.217 keV/μm at a depth of 17.7 cm (a few mm before the average range for 76-MeV pions). The spectra shown in Fig. 2 are measured for range-shifted beams, and therefore, the primary particle contributions will be a combination of distributions for narrow (unmodulated) beams with various ranges. The energy events which peak around 1 keV/μm are associated with pions, muons, and electrons. Their contribution extends to higher lineal energies (y), although in an exponentially decreasing manner. Neutrons, protons, and heavier particles are produced by in-flight pion interactions and absorption of pions at rest. The first process produces particles distributed relatively uniformly in the water phantom, while the latter results in highly localized energy depositions which are correlated to the shape of the pion stopping distribution. A detailed unfolding of the spectra in terms of particle types requires a knowledge of the energy distributions at every point in the treatment field. This information is generally not available. Based on previously measured distributions for various particles(6) and the known maximum (and possibly minimum) stopping power for each type of particle, some estimates can be made. Protons are expected to deposit energies up to about 140 meV/μm with a peak around 4 keV/μm (see Fig. 2). The decrease around 400 keV/μm can be associated with maximum lineal energy for alpha particles. Higher energies correspond to heavier nuclei, although distinct edges are hard to observe because of the limited number of events. Important contributions come from neutrons, mainly via (n,p) reactions and they will increase the proton and heavier ion components. Photons will alter the electron spectrum through the photoelectric effect, pair production and Compton scattering processes. An important characteristic of the indirectly ionizing secondaries is their relative diffuseness and relative homogeneity in space as compared with the primary charged reaction products. Finally, δ-rays associated with energetic charged particles will modify the lower lineal energy part of the spectra.

The relative shape of the two spectra in Fig. 2 can be understood if one considers the way in which the dose is delivered at the two extreme positions of the broad peak. At the proximal part of the peak (8 cm) comparable amounts of passing pions (which stop further downstream) and stopping pions are present. The spectrum at the distal edge of the peak (16 cm) is dominated by stopping pions, with a minimal contribution from the remaining low-energy passing pions. The amount of muon-electron contaminants at both positions is about the same, as no significant change occurs in their fluence along the 10 cm pion peak. The most manifest effect observed in the two spectra is the dramatic increase at higher y (at 16 cm) with a corresponding decrease at lower y. This effect can be seen also if one compares the dose and frequency means for the two positions: at 8 cm y_F = 0.7 keV/μm, y_D = 19 keV/μm; at 16 cm y_F = 1.2 keV/μm, y_D = 61 keV/μm. In order to further elucidate the origin of these changes, a comparison is made in Fig. 3 between the 16 cm spectrum and a spectrum obtained previously (see Ref. 2) at the distal edge of a narrow beam peak. The pion contributions to these spectra ought to be similar because the relative number of stopping pions is nearly the same. In fact, the data show that the spectrum for the broad beam has more events at higher lineal energies. (The differences at lower energies are partially a result of different electron-muon contamination.) There are two factors which could contribute toward this difference: 1) the broad beam has contributions from the other overlapping narrow beams as a result of the range-shifting process, and 2) there is a significant change in the neutron contribution in the broad beam resulting from its modulated character.

The contribution of the first factor was found to be minimal by calculating a new microdosimetric distribution through an appropriate folding of narrow beam distributions according to the range-shifter movements (see Fig. 3). As expected, no important change is observed as compared to the single narrow beam distribution discussed before. In the following, a tentative explanation of these differences is advanced.

Pion stars produce an average of 2 neutrons per stopped pion. We estimate from the experimental data of Amols, et al.,[(9)] similar unpublished data for broad beams by the authors, and the calculations of Schillaci and Roeder[(10)] that the fraction of neutron dose is approximately twice as large in the broad beam as compared to the narrow beam. As mentioned previously, because of their long mean free paths, neutrons are poorly correlated, in space, with the pion beam. As a consequence of this, the neutron distribution throughout the peak region will be relatively less sensitive to the range-shifting process. The fact that in a broad beam the same number of stopping pions is spread over a larger volume (i.e., less pions per unit volume), together with the relative constant neutron flux irrespective of the pion beam shape, indicates that for <u>equal</u> doses, broad beams will have an increased neutron contribution as compared to narrow beams. This contribution effectively suppresses the expected trend of decreasing mean lineal energy for the charged particles as the stopping volume increases. Similar effects for electrons and muons will reduce the mean lineal energies in the peak. The observed results are a combination of all these factors. The immediate consequence of these effects is that any calculational procedure to obtain broad beam distributions from narrow beam spectra should make use of the neutron, electron, and muon distributions (as opposed to the pion associated spectra) in order to include them correctly. Further experiments to test this hypothesis are now in progress at LAMPF.

In Fig. 4 the fraction of dose in excess of a given y-value for the measured pion spectra is compared with data for high energy neutrons[11] and data for 557 MeV/amu Ne ions (see Ref. 8) obtained in the middle of a broad Ne beam. In the energy region of 10^0 to 10^2 keV/μm, 16 cm pions and the neutrons are quite similar. The Ne data are dominated by the large amount of dose delivered around 50 keV/μm at higher lineal energies. Pions at 16 cm deliver the largest fraction of the dose. This is a direct reflection of the effects described previously.

For comparative purposes, RBE and OER values have been calculated for mammalian cells at 50% survival with the Theory of Dual Radiation Action.[4] Using the narrow beam and the 8 cm and 16 cm broad beam data, one obtains values for the RBE of 1.17, 1.09, and 1.26, respectively. The OER is approximately 1.6 for all three spectra. No attempt was made in the present paper to fit these values to available biology data. The RBEs follow in general the trend expected from the $\bar{y}_D$ values for these beams. Their relative values, though, may vary significantly if one changes the saturation parameter, y_o (see Ref. 4) which was chosen to be 125 keV/μm in the present calculation. No measured values of y_o for pion fields and for specific biological systems are available to date. The significance of increased contributions from high y-values in the 16 cm beam is, therefore, a function of where the "overkill" effect begins to occur for pions (i.e., the y_o value).

CONCLUSIONS

Microdosimetric measurements have been performed for a broad, therapeutical negative pion beam. It has been proposed that microdosimetric spectra for broad beams can be calculated from the experimental spectra for narrow beams. The process of range-shifting the beam alters the radiation quality of the beam in a manner which depends strongly on the spatial and energy distribution of various components (neutrons, electrons, muons) of the original, unmodulated beam. Consequently, additional knowledge of these components, not available from the usual microdosimetric measurements, is necessary in order to incorporate in treatment planning information concerning the radiation quality. Calculations of the biological response resulting from these physical changes have been performed for specific systems and will be reported elsewhere. The uncertainties associated with the present biological data and the limitations of the available models make it difficult to estimate the importance of these effects for patient treatments.

REFERENCES

1. M.M. Kligerman, G. West, J.F. Dicello, C.J. Sternhagen, J.E. Barnes, K. Loeffler, F. Dobrowolski, H. T. Davis, J.N. Bradbury, T.F. Lane, D. F. Petersen, and E.A. Knapp, "Initial Comparative Response to Peak Pions and X rays of Normal Skin and Underlying Tissue Surrounding Superficial Metastatic Nodules,"Amer. J. of Roent. 126: 261-267, 1976.

2. J.F. Dicello, P. Fessenden, and R.M. Henkelman, "Dosimetry of Beams for Negative Pi-Meson Radiation Therapy," Int. J. Radiat. Oncology Biol. Phys. 3, 299-306 (1977) and references therein.

3. A.C. Lucas, W.M. Quam, and M.R. Raju. 1969. "Microdosimetry for a Pi-Meson Beam," EG&G Technical Paper S-54-TP.

4. M. Kellerer, and H. Rossi, "The Theory of Dual Radiation Action," Current Topics in Radiation Research Quarterly 8, 85-158 (1972).

5. M. Paciotti, Los Alamos Scientific Laboratory, private communication.

6. H.I. Amols, D.J. Liska, and J. Halbig, "The Use of a Dynamic Range-shifter for Modifying the Depth Dose Distributions of Negative Pions," Med. Physics, Vol. 4,No. 5 (Sept/Oct 1977) pp 404-407.

7. M. Zaider, J.F. Dicello, and R.D. Hiebert, "A Pulsed System for Obtaining Microdosimetric Data with High Intensity Beams," IEEE Trans. on Nucl. Sci. NS-25, 202-204 (1978).

8. J.F. Dicello, and M. Zaider, "Microdosimetry for Pedestrians: An Introduction," Los Alamos Scientific Laboratory Report
Presented at the AAPM Charged Particle Beam Task Group Workshop, Los Alamos, NM March 1978.

9. H.I. Amols, J. Bradbury, J. Dicello, J. Helland, M. Kligerman, T. Lane, M. Paciotti, D. Roeder, M. Schillaci, "The Dose Outside of the Treatment Volume for Patients Irradiated with Negative Pions," Phys. in Med. & Biol. Vol. 23 (3) pp 385-396 (1978).

10. M.E. Schillaci, and D.L. Roeder, "Dose Distributions Due to Neutrons and Photons Resulting from Negative Pion Capture in Tissue," Phys. Med. Biol. 18, 821-829 (1973).

11. H.I. Amols, J.F. Dicello, M. Awschalom, L. Coulson, S.W. Johnsen, and R.B. Theus, "Physical Characterization of Neutron Beams Produced by Protons and Deuterons of Various Energies Bombarding Beryllium and Lithium Targets of Several Thicknesses," Med. Phys. 4, 486-493 (1977).

FIGURE CAPTIONS

Fig. 1 General layout of the experimental setup.

Fig. 2 Microdosimetric distributions obtained in the present experiment at depths of 8 and 16 cm below the water level. The abscissa represents the lineal energy y which is defined as the energy of an event divided by the mean chord length of the active volume (2/3 the simulated diameter). The ordinate is the product of y and the dose distribution, $d(y) = yf(y)$, where $f(y)$ is the frequency distribution in y. The insert shows the absorbed dose as a function of depth in water along the central axis. The positions where the microdosimetric spectra have been obtained are indicated by arrows.

Fig. 3 Comparison of the 16-cm data (present experiment), narrow beam data (Ref. 2) and a spectrum calculated with the range shifter function and narrow beam data. The representation is the same as that used in Fig. 2.

Fig. 4 Integral dose distributions, $1-D(y)$, as a function of y. The quantity $[1-D(y)]$ is the fraction of dose delivered in excess of a given y. The present data are compared with similar data for a broad neon beam (Ref. 8), and a high energy neutron beam (Ref. 11).

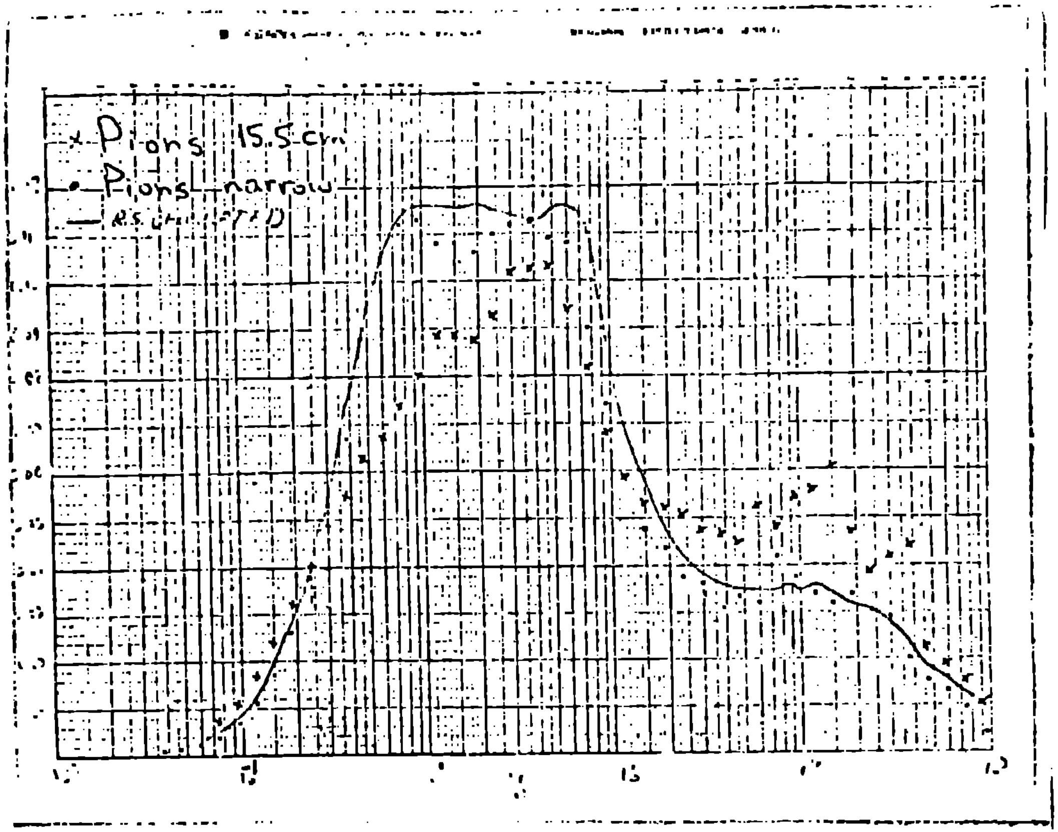
x Pions 15.5 cm
• Pions narrow

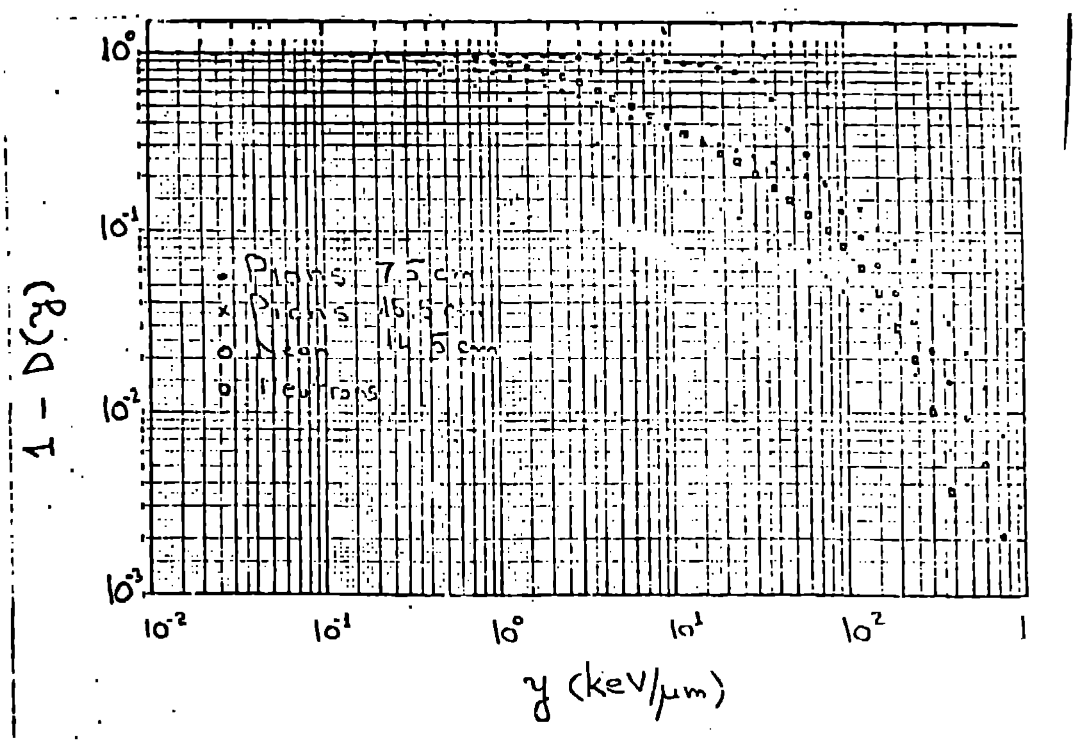
1 - D(y)
10⁰
10⁻¹
10⁻²
10⁻³
• Pions 7.5 cm
x Pions 15.5 cm
o Neon 14.5 cm
□ Neutrons
10⁻²
10⁻¹
10⁰
10¹
10²
y (keV/μm)

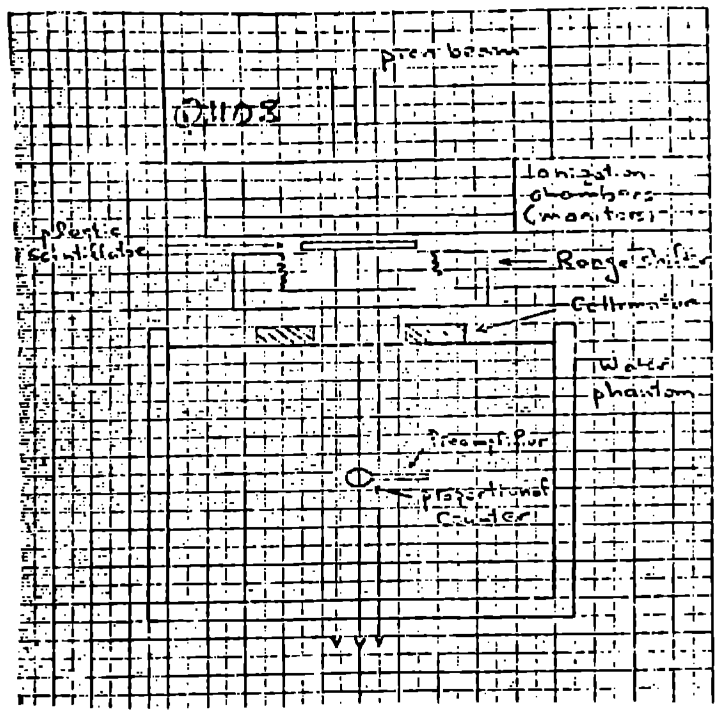
proton beam
Ionization chambers (monitors)
Plastic scintillator
Range shifter
Collimator
Water phantom
Preamplifier
proportional counter

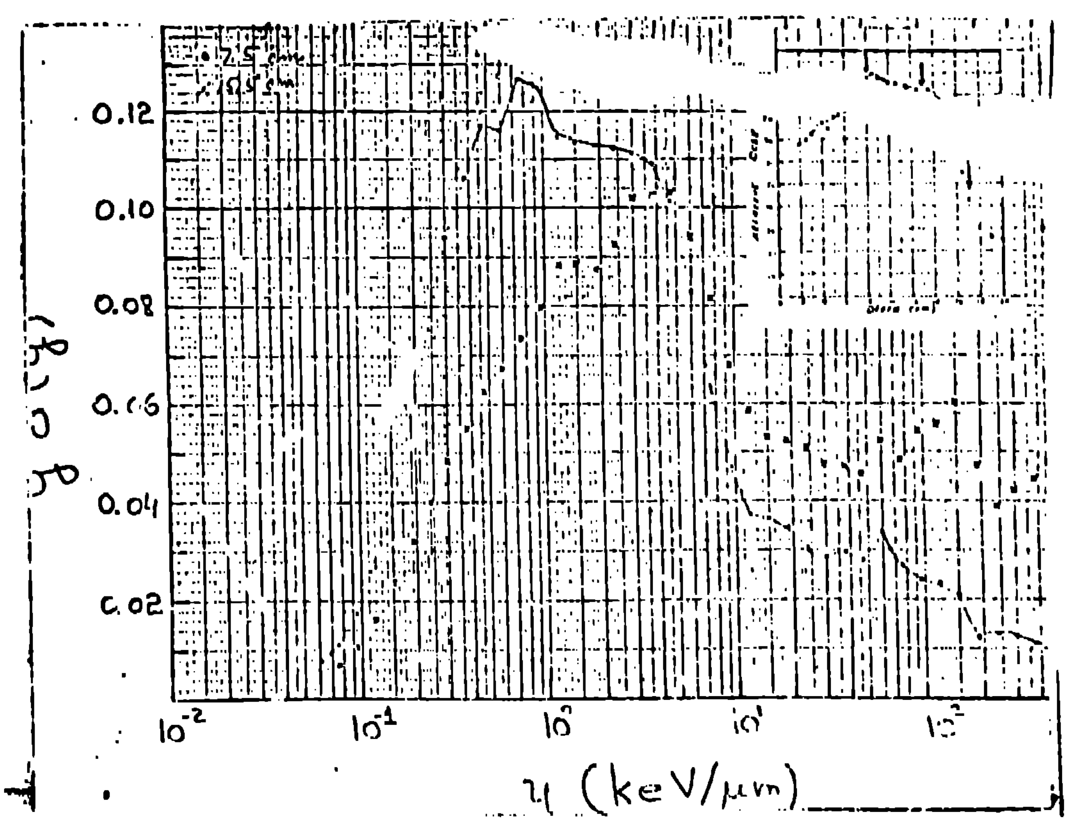
0.12
0.10
0.08
0.06
0.04
0.02
10^{-2}
10^{-1}
10^{0}
10^{1}
10^{2}
y (keV/μm)